High-throughput generation of bispecific binding proteins by sortase a-mediated coupling for direct functional screening in cell culture

Andres, Fabio; Schwill, Martin; Boersma, Ykelien L.; Plückthun, Andreas

Published in:
Molecular cancer therapeutics

DOI:
10.1158/1535-7163.MCT-19-0633

Publication date:
2020

High-Throughput Generation of Bispecific Binding Proteins by Sortase A–Mediated Coupling for Direct Functional Screening in Cell Culture

Fabio Andres[1], Martin Schwill[1], Ykelien L. Boersma[1,2], and Andreas Plückthun[1]

ABSTRACT

High-throughput construction of multivalent binders and subsequent screening for biological activity represent a fundamental challenge: A linear increase of monovalent components translates to the square of possible bivalent combinations. Even high-efficiency cloning and expression methods become limiting when thousands of bispecific binders need to be screened for activity. In this study, we present an *in vitro* method for the efficient production of flexibly linked bispecific binding agents from individually expressed and purified monovalent binders. We established a sortase A–mediated coupling reaction to generate bispecific designed ankyrin repeat proteins (DARPins), with an optimized reaction maximizing the bivalent coupling product with low levels of monovalent side-products. These one-pot reaction mixtures could be used directly, without further purification, in cell-based assays. We generated a matrix of 441 different bispecific DARPins against the extracellular domains of the cancer-associated receptors EGFR, ErbB2, ErbB3, ErbB4, EpCAM, and c-MET and screened on two different ErbB2-positive cancer cells lines for growth-inhibitory effects. We identified not only known but also novel biologically active biparatopic DARPins. Furthermore, we found that the cancer cell lines respond in a highly reproducible and defined manner to the treatment with the 441 different bivalent binding agents. The generated response profiles can thus be used for functional characterization of cell lines because they are strongly related to the cell line–specific surface receptor landscape. Thus, our method not only represents a robust tool for screening and lead identification of bispecific binding agents, but additionally offers an orthogonal approach for the functional characterization of cancer cell lines.

Introduction

Multivalent, multidomain, and multispecific binding proteins are commonly found in nature (1), where they regulate the spatial and temporal proximity of thousands of protein–protein interactions (2). Thereby, they control various signaling cascades by binding to their targets. Consequently, multivalent binding proteins, such as adaptor or scaffold proteins, enable specific signaling events between their target proteins while preventing others. This specificity is encoded in their primary sequence (3), and overexpression of particular multivalent adaptor proteins is known to induce oncogenic transformation (4). Similarly, extracellular growth factors such as hepatocyte growth factor (HGF; ref. 5) or FGF (6) are prominent proto-oncogenes, which stimulate the activation of receptor tyrosine kinases (RTK) through intermolecular bridging and stabilization of the RTK–dimer interactions, which are found frequently upregulated in various types of cancers and are associated with the development of cancer drug resistance (6, 7).

In contrast, the majority of approved therapeutic proteins are binding agents directed against a single target (8, 9). Typical monospecific therapeutic IgGs, the most widely used protein therapeutics, show limited functionality for connecting, or separating, multiple different target antigens on the cell surface (10). While the IgG scaffold represents a proven approach for the development of targeted cancer therapies, typically involving its Fc-mediated effector functions, this strategy may be insufficient by itself. It has become evident that IgG-based therapies can suffer from low effectiveness due to the emergence of cancer drug resistance (11–13).

Therefore, the field of multispecific binding proteins with versatile functionalities has emerged over the past decade, starting with bispecific antibodies (14, 15), but more recently also employing other scaffolds, which aim to overcome the limitations set by the IgG format (16). A particularly suitable tool to generate multivalent binding proteins is represented by robust alternative binding proteins such as designed ankyrin repeat proteins (DARPins; ref. 17). They show, next to very high thermal stability, very high target specificity and the ability to easily generate multivalent fusion proteins of many formats. Such multivalent binding proteins convey increased avidity through simultaneous binding to multiple target antigens, with geometry that can be widely adjusted. These multivalent binding agents can be composed of copies of the same paratope (classic bivalent or multivalent binder), or different paratopes directed against distinct epitopes on the same molecule (biparatopic binders), or paratopes directed against two different molecules (classic bispecific binders). Besides increasing avidity, and perhaps cell selectivity, multispecific binding molecules may also induce completely novel mechanisms of action. By linking surface receptors in signaling-inactive orientations, cancer growth signaling can be efficiently disrupted (18). This effect can be superior to that of a simple mixture of conventional IgGs against the same epitopes and, therefore, these multispecific molecular formats represent a promising alternative to conventional IgGs. The challenge, however, is to find such biologically active bispecific molecules. In most

[1]Department of Biochemistry, University of Zurich, Winterthurerstrasse, Zurich, Switzerland. [2]Department of Chemical and Pharmaceutical Biology, Groningen Research Institute of Pharmacy, University of Groningen, Groningen, the Netherlands.

Note: Supplementary data for this article are available at Molecular Cancer Therapeutics Online (http://mct.aacrjournals.org/).

F. Andres and M. Schwill contributed equally to this article.

Corresponding Author: Andreas Plückthun, University of Zurich, Winterthurerstrasse 190, 8057 Zurich, Switzerland. Phone: +41-44-635-5570; Fax: +41-44-635-5712; E-mail: plueckthun@bioc.uzh.ch

Mol Cancer Ther 2020;19:1080–8

doi: 10.1158/1535-7163.MCT-19-0633

cases, the monomeric components from which they are built will be inactive, such that the active bispecific molecules need to be found with high efficiency in high-throughput screenings.

Biparatopic binding agents have been shown to induce internalization of EpCAM (19), internalization and degradation of EGFR (20), or cause an intermolecular cross-linking of ErbB2 that uncouples the receptor from all signaling (18, 21). In a different mode of action, combined inhibition of EGFR and ErbB3 was achieved (22).

In all of these cases, these activities were only observed in the bispecific formats (or at least much more potent), while even the combination of the monovalent binders was essentially inactive. These biparatopic binding agents were discovered through screening strategies, usually after rational optimization of the constructs to minimize the number of possible binder permutations to be tested; still, these strategies do require profound knowledge of the target's structure and function. For the large majority of cell surface receptors as well as the plethora of potential cross–family interactions, however, different approaches are required: detailed knowledge of the target may not be available at present. In this study, we present an innovative screening method for the identification of novel biologically active multispecific binding proteins in high throughput.

Previously, we reported DARPins binding to EGFR, ErbB2 and ErbB4 (23–25), EpCAM (19), and c-MET (26), which were selected either by phage or ribosome display. Here, we introduce and add to the collection novel DARPins derived from ribosome display selections against the extracellular domain of ErbB3. From binders to these targets, we chose 20 different DARPins of N2C or N3C format (17) that showed high target selectivity, low-nanomolar to picomolar binding affinities, and monomeric behavior in size-exclusion chromatography. Using these monovalent DARPins, we developed a one-pot coupling reaction using the *Staphylococcus aureus* transpeptidase sortase A (27, 28) to robustly generate covalently fused bivalent molecules in a scalable format. DARPin off7 targeting *Escherichia coli* maltose-binding protein (29) was used as a nonbinding control; finally, we fused 21×21 DARPins to obtain 441 different bispecific binding molecules. The one-pot coupling reaction and the subsequent *in vitro* screening did not require the genetic construction and expression of the individual bivalent binders; it did not require additional purification steps after coupling and the bivalent binding agents were fused covalently. Altogether, this provides several benefits over previously reported large-scale screening approaches for bispecific proteins (30, 31). We directly screened for the biological effect of the bispecific constructs on $HER2^+$ cancer cell lines in high-throughput cell viability assays, and we identified a set of novel bispecific DARPin molecules that can either block cancer cell proliferation or, conversely, significantly stimulate it. We rediscovered previously reported active biparatopic DARPin constructs, which serve as an internal assay control, and discovered bivalent binders with strong biological effects confirming the robustness of this technology.

Materials and Methods

Cell lines and reagents

Human carcinoma cell lines BT474, SKBR3, and A549 were obtained from the ATCC (www.atcc.org) and cultured in RPMI1640 medium from Life Technologies with 1% (v/v) penicillin/streptomycin from Sigma Aldrich and 10% (v/v) FCS from BioConcept. Protease inhibitors pefabloc from Merck, leupeptin and pepstatin from Serva and marimastat from Calbiochem were used for Western blot analysis. Antibodies against EGFR (D38B1; #4267), ErbB3 (D22C5; #12708), EpCAM (D1B3; #2626) were purchased from Cell Signaling Technology, ErbB2 (3B5; OP15) from Calbiochem, and GAPDH (sc-365062) from Santa Cruz Biotechnology. The polyclonal anti-DARPin serum was produced in-house. The anti-myc antibody (9E10) was obtained from Sigma. Secondary anti-mouse IgG IRDye800 conjugate from Rockland (610-732-124) and anti-rabbit IgG Alexa680 (A-21109) from Invitrogen were used for IR-Western blot detection on an Odyssey system from LI-COR.

Ribosome display selection and characterization of ErbB3-binding DARPins

DARPin libraries in N2C and N3C format were used to select binders targeting the ErbB3 ectodomain (residues 20-500, produced as an Fc-fusion protein). Four rounds of selection by ribosome display were performed as described previously (32). In each round, the translation mixture was incubated for 1 hour at 4°C with 100 nmol/L chemically biotinylated ErbB3 in solution; complexes bound to ErbB3 were captured using streptavidin-coated paramagnetic beads. Selection stringency was increased in each round by additional washing steps. The DNA output from round four was subcloned into the vector pQE30 and used for transformation of *E. coli* XL1-Blue; single-selected DARPins were expressed in 96-well format and screened for binding in ELISA (23). The top ten binders were sequenced, produced in 1 L *E. coli* XL1-Blue cultures, and purified via their N-terminal $MRGSHis_6$-tag using Ni-NTA Resin (Qiagen) according to standard procedures (23). Finally, the ErbB3-DARPins were characterized on the basis of their affinity and specificity using ELISA.

To recover binders recognizing different epitopes, three additional rounds of ribosome display were carried out using the N2C DARPin library while masking the dominant epitope of DARPin F3 (100 nmol/L). The DNA output from round three was subcloned into the vector pQIq and *E. coli* XL1-Blue was transformed; single DARPins were expressed in 96-well format and screened for binding in ELISA (23). The top four binders were again sequenced, produced in 1 L *E. coli* XL1-Blue cultures, and purified using Ni-NTA resin. Binders were characterized as above.

Production of sortase A and TEV protease

S. aureus sortase A wild-type (wtSrtA), its pentamutant (P94R/D160N/D165A/K190E/K196D; ref. 33), and TEV protease were produced from standard bacterial expression plasmids (pQE30-derivatives) in 1 L cultures of *E. coli* XL1-Blue cells using LB medium. Cells were lysed by sonication and French press, and the cleared and filtered supernatant was applied to Ni-NTA immobilized metal affinity chromatography (IMAC) for purification of His-tagged proteins. In the case of TEV protease, all purification steps were carried out in the presence of 4 mmol/L *2*-mercaptoethanol. Sortase A and TEV enzymes were dialyzed against HBS_{150} (20 mmol/L HEPES pH 7.5, 150 mmol/L NaCl) and aliquoted.

Construction, production, and purification of "sortaggable" DARPins

For the generation of DARPins bearing the peptide extensions needed for enzymatic coupling by sortase A, 21 DARPin sequences were each inserted by restriction cloning via *Bam*HI and *Hind*III into the multiple cloning site of both pQIq_MRmyc_LPETG_His_6 and pQiBi_His_6_TEV_Gly_5. The resulting 42 constructs were expressed in 1.5 L cultures of *E. coli* BL21(DE3) cells using 2YT medium. Cells were lysed by a continuous flow cell disruption system (Constant Systems Ltd). Cleared and filtered supernatants were applied to IMAC purification using Ni-NTA (Qiagen Superflow resin) including additional washing with 60–80 column volumes PBS containing 0.5% (v/v)

Triton X-114 (Sigma-Aldrich), followed by 50 column volumes of cell-culture grade PBS for removal of bacterial endotoxins. After elution, buffer was exchanged to HBS_{150} by dialysis, DARPins were aliquoted and stored at −80°C.

Sortase A catalyzed DARPin–DARPin transpeptidation

Coupling of DARPins was performed in a one-pot reaction, containing final concentrations of 40 μmol/L of each DARPin educt (DARPin-LPETG, G_5-DARPin), 0.5 μmol/L TEV protease, 3 μmol/L wtSrtA (or penta-mutant SrtA in the test reactions), and 10 mmol/L $CaCl_2$ in HBS_{150} buffer. DARPins were prediluted to working stocks of 200 μmol/L. High-throughput coupling of 21 × 21 combinations was performed in 96-well plates, applying both enzymes and $CaCl_2$ as a master mix before the individual DARPin solutions were added from the prepared working stocks. Reactions had a final volume of 120–200 μL and were incubated for 2 hours at 25°C and subsequently overnight at 4°C on an orbital shaker. Twenty-eight random samples were analyzed by SDS-PAGE for coupling efficiency.

Size-exclusion chromatography

Size-exclusion chromatography (SEC) was performed in HBS_{150} buffer on an ÄKTA Pure system using a Superdex 200 30/300GL column with a flow rate of 0.5 mL/min (GE Healthcare).

High-throughput receptor cross-linking and cell viability assay

Multiwell plates were loaded with a semiautomated pipettor system CyBio SELMA (Analytik Jena). A total of 1,200 cells were seeded 24 hours prior to treatment in 25 μL RPMI1640 medium supplemented with antibiotics (penicillin/streptomycin) and 10% (v/v) FBS from Amimed (BioConcept) into Falcon clear TC-treated 384-well microplates (Corning). Coupling reactions were diluted in HBS_{150} prior to proliferation assays such that final dilutions of 40-, 160-, and 640-fold were obtained in the assay. Five microliters of each prediluted coupling reaction was transferred to viability assay plates ($n = 3$). As controls, 5 μL of HBS_{150}, mock reaction mixture (no DARPins), and monomeric DARPins were added to plates. Multiwell plates were incubated in humidified incubators at 37°C for 4 days. On day 5, 25 μL of a 1:1 mixture of XTT reagent (Cell Proliferation Kit II, Roche) with serum-free RPMI medium was added to the wells and plates were incubated for up to 5 hours at 37°C. Absorbance at 450 nm was measured on a Tecan Infinite M1000 Microplate Reader (Tecan). Background signals of control wells (no cells) were subtracted from the raw absorbance data per plate.

Data analysis

For Pearson correlation, the mean of three dilutions (each measured in triplicate, total of $n = 9$) was transformed to $\log_2$-fold changes (LFC) versus untreated cells. *P* values were calculated by two-sided Student's *t*-test versus mock binding control DARPin off7-off7 ($n = 9$). Pearson correlation coefficients and heatmaps were made in Perseus (Max-Planck Institute of Biochemistry, Germany).

Results

Selection and characterization of ErbB3-binding DARPins

To complement our portfolio of binders against tumor surface markers to be used in the generation of bispecific constructs, we selected binders against ErbB3. After each round of ribosome display selection, the captured mRNA was reverse-transcribed to DNA. Surprisingly, after the third round no enrichment of N3C binders was observed; therefore, only the N2C library was used further in a fourth round of selection. Single N2C DARPins from round four were screened for binding in ELISA; this yielded ten binders with different sequences, and from this set DARPins A1 and F3 were selected for further studies. Both DARPins bound with high specificity to ErbB3 ECD (Supplementary Fig. S1A), and F3 competed for binding with the ErbB3 ligand heregulin (Supplementary Fig. S1B). Both DARPins bound with nanomolar affinity to ErbB3 ECD (A1, ca. 12 nmol/L and F3, ca. 40 nmol/L).

Because most selected binders belong to the same family, and must therefore bind to the same or overlapping epitopes, we carried out new selections masking this favored epitope by addition of 100 nmol/L of purified DARPin F3. Only the N2C library was used as input for this selection. After three rounds of selection, four different binders were selected; and for this study, binder C7x was chosen. C7x was found to be specific for ErbB3, showed an affinity of ca. 85 nmol/L (Supplementary Fig. S2A), and, as expected, did not compete for binding with heregulin (Supplementary Fig. S2B).

Development of the one-pot coupling reaction

A summary of the one-pot enzymatic coupling reaction and subsequent analysis by *in vitro* cell-based assays is shown in **Fig. 1A**. Monovalent DARPins were expressed individually, purified, and afterwards enzymatically conjugated using the bacterial transpeptidase sortase A (SrtA; ref. 34), resulting in a flexibly linked bivalent fusion protein. SrtA catalyzes the formation of a covalent peptide bond between two proteins in a two-step reaction (27). Briefly, the N-terminal DARPin educt bears the SrtA recognition sequence, LPETG, at its C-terminus and is referred to as DARPin-LPETG. SrtA binds to the LPETG motif and cleaves the Thr-Gly peptide bond, forming a covalent acyl–enzyme intermediate. In a second step, this acyl–enzyme intermediate is attacked by the nucleophilic amino group of the N-terminal Gly from a second DARPin educt (which will become the C-terminal unit), referred to as G_5-DARPin (carrying 5 Gly residues at the N-terminus), whereupon SrtA is released and the two DARPins are site-specifically coupled via a new Thr-Gly peptide bond.

For scalable expression and purification, all G_5-DARPins were expressed as precursor constructs (MRGS-His_6-TEV-GGGGG-DARPin). A free N-terminal Gly-tag was generated by TEV protease cleavage within the one-pot reaction, as schematically depicted (**Fig. 1A**). Importantly, the conditions of the coupling reaction were optimized for application in a 96-well format: this enabled subsequent functional screening of the bispecific binders for biological effects in the *in vitro* cell-based assays (**Fig. 1B**), without the need for prior purification.

Because noncoupled monovalent binders could potentially interfere with the bivalent binding in the cell-based assays and might therefore mask any biological activity of the bivalent molecules, we optimized the protocol to generate the maximum ratio of bivalent product over noncoupled monovalent binders. For this purpose, we compared the activity of wtSrtA directly to that of an evolved SrtA mutant. This SrtA pentamutant was previously selected by yeast display for faster turnover rates using short peptide educts at millimolar concentrations (33). After enzymatic coupling using the evolved pentamutant of SrtA, we observed *higher* accumulation of monovalent DARPin side products (**Fig. 2A**) in comparison with the same reactions with wtSrtA.

In our system, the sortase needs to catalyze the coupling of low-micromolar concentrations of the substrates. Presumably, in the case of the pentamutant, the DARPin–LPET–enzyme intermediate is not attacked by the amino terminus of the C-terminal coupling partner at a

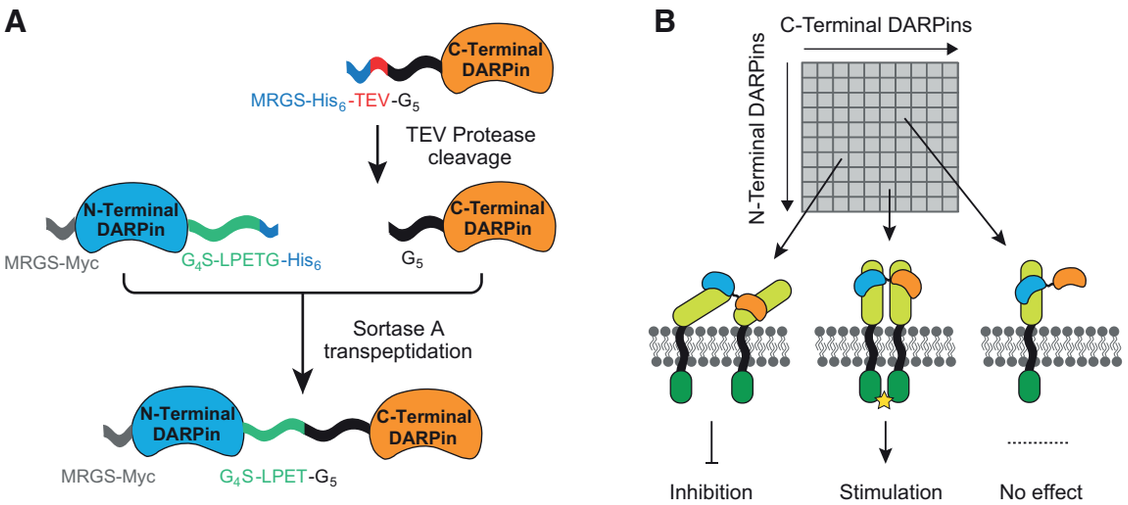

Figure 1.
Scheme of bivalent DARPin generation and screening in receptor cross-linking and proliferation assays. **A,** The one-pot coupling reaction involves two different enzymatic steps: (i) cleavage of the N-terminal MRGS-His_6 sequence from the C-terminal coupling partner by TEV protease and (ii) the transpeptidation reaction by SrtA. **B,** Concept of the combinatorial bispecific binder matrix. Bispecific DARPins derived from the high-throughput coupling reaction were used directly for screening of their receptor-binding effects in the cell-based assay. Here, we distinguish between the three possible effects on cell proliferation: inhibition, stimulation, and nonsignificant effects.

sufficiently fast rate to completely avoid nonspecific hydrolysis, releasing a cleaved DARPin-LPET product (**Fig. 2A**) from the acyl–enzyme intermediate. Applying the G_5-DARPin in a 2-fold molar excess slightly increased the amount of total-formed conjugation product; however, the hydrolyzed side product still accumulated to a high extent. Moreover, the hydrolyzed side product accumulated over time, accompanying a reduction of total bivalent product. This presumably reflects the ability of the evolved SrtA pentamutant to also recognize

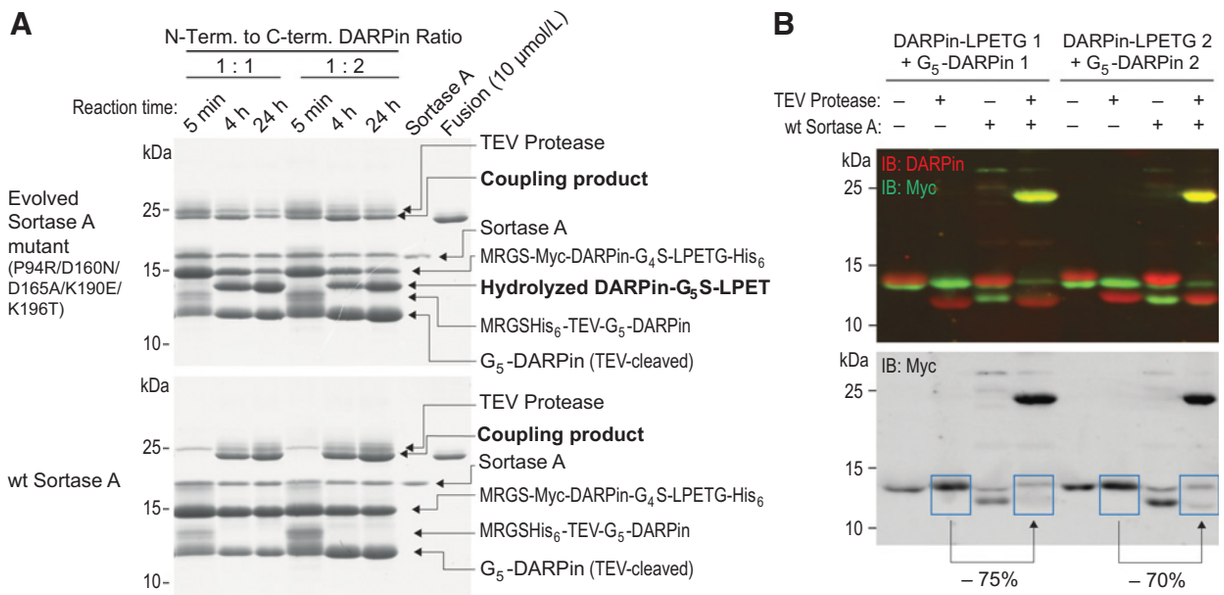

Figure 2.
Method development and optimization of enzymatic DARPin–DARPin coupling. **A,** SDS-PAGE of reaction mixes after different incubation time points to compare ratios of monovalent substrate DARPins with the bivalent DARPin products between the SrtA pentamutant (top) and wtSrtA-mediated coupling (bottom). **B,** Analysis of coupling reactions after 24-hour incubation by two-color IR immunoblotting (IB; top) and quantification of coupling efficacy by detecting Myc-tag signal reduction of the monovalent N-terminal DARPin (bottom). Note that while the simultaneous detection of the bivalent construct by anti-DARPin serum and N-terminal myc-tag detection leads to a yellow signal, in the monovalent case, the stronger green from the myc-tag dominates, as proportionally fewer (red) antibodies can bind to the monovalent DARPin.

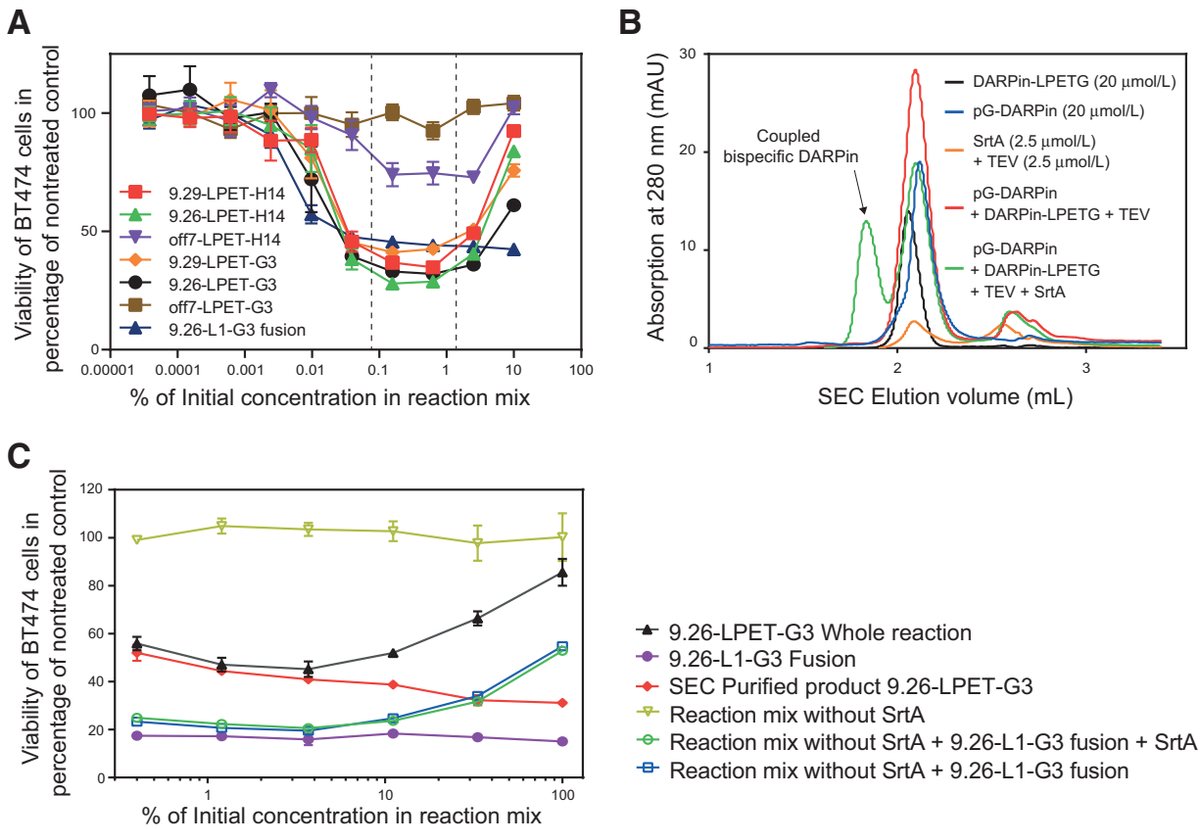

Figure 3.

Development and optimization of the cell XTT cell viability assay for the analysis of the one-pot coupling reaction. **A,** Biological effects of serial dilutions of whole coupling reaction mixtures on BT474 cells after 4 days of treatment. Each data point represents the mean of triplicates with standard deviation, normalized to a nontreated control. **B,** SEC profiles at 280 nm absorbance of a coupling reaction and its components. **C,** Biological effect of serial dilutions of coupling reactions, purified coupling product, and genetically fused controls on BT474 cells after 4 days of treatment. Each data point represents the mean of triplicates with SD, normalized to a nontreated control.

the LPETG motif within the linker of the coupled product, enabling further hydrolysis due to its improved kinetics—obviously an unwanted reaction. The wtSrtA, on the other hand, showed a slower accumulation of the desired coupling product without the formation of side products over time (**Fig. 2A**), consistent with a much slower (or absent) hydrolysis of the end product. Here, an excess of G_5-DARPin over DARPin-LPETG slightly increased the amount of bivalent product; nevertheless, the overall ratio of coupled to noncoupled species remained similar or even less favorable.

To determine the efficiency of the coupling reactions, we performed quantitative immunoblotting with infrared (IR) detection. **Figure 2B** shows two randomly chosen DARPin-coupling reactions before and after the addition of enzymes (wtSrtA and TEV protease), probed with an antibody against the N-terminal myc-tag of the DARPin-LPETG (top blot, green channel) and a polyclonal anti-DARPin serum (top blot, red channel). Upon addition of TEV protease, we observe a 2 kDa downshift of the G_5-DARPin band (red) due to the removal of the MRGS-His_6-TEV peptide-tag. Next, the sole addition of SrtA to the substrates, without any addition of TEV protease, resulted in the accumulation of a hydrolyzed DARPin-LPET (at ca. 12 kDa)—it cannot be attacked by the other DARPin in the absence of a free GGG N-terminus—as well as some minor nonspecific cross-linked species of high molecular weight. Upon combination of both enzymes in the reaction mix, the desired bispecific DARPin product is efficiently formed (~24 kDa, yellow band). While the simultaneous detection of the bivalent construct by anti-DARPin serum and N-terminal myc-tag detection leads to a yellow signal, in the monovalent case, the stronger green from the myc tag dominates, as proportionally fewer (red) antibodies can bind to the monovalent DARPin. We therefore based our coupling quantification on anti-myc-tag signal reduction in DARPin-LPET(G), which revealed a coupling efficacy of about 75% (**Fig. 2B**, bottom blot).

As a benchmark within the development of the method, we used the apoptosis-inducing biparatopic DARPins against ErbB2 (consisting of combinations of the DARPins 9.26, 9.29, G3, and H14; ref. 21) to treat the ErbB2-addicted cancer cell line BT474. We analyzed serial dilutions of the reaction mixtures after enzymatic coupling and compared them directly to the genetically fused construct (9.26-L1-G3; ref. 21) in a cell viability assay (**Fig. 3A**). We detected a marked inhibition of cell viability between a dilution of 1/100 to 1/10,000 of the initial reaction mix after 4 days of treatment. Using 40 µmol/L of each of the monovalent DARPin educts and assuming a coupling efficiency of about 70%, this dilution range corresponds to a final concentration of the coupled bispecific product between 3 nmol/L (at a dilution of 1/10,000) and 300 nmol/L (at 1/100). This is in good agreement with previously determined IC_{50} values of biparatopic anti-ErbB2 DARPins

with long linkers (21) and also with the behavior of the genetically fused positive control 9.26-L1-G3.

On the other hand, at lower dilutions of the initial coupling reactions (higher concentration of reaction mix in the cell assay), we observed a striking loss of inhibitory activity in the XTT assay. At 10-fold dilution, the antiproliferative effect was mostly lost, whereas as previously shown the purified fusion 6L1G retained its maximum antiproliferative activity. We speculated that the loss of activity at lower dilutions of the reaction mixtures might be related to the higher total concentrations of uncoupled monomeric educt DARPins, which have K_D values in the pmol/L and low nmol/L range, respectively. To test this hypothesis, we performed a coupling reaction at a larger scale and separated the coupled fraction by SEC as shown in **Fig. 3B**. The formation of the coupled DARPin–DARPin product can be followed by the peak formation at a lower elution volume of approximately 1.9 mL in the reaction containing the DARPin educts and both enzymes. The peaks at approximately 2.7 mL elution volume with smaller absorption value consists of, in the respective reactions, the SrtA enzyme itself, as well as MRGS-His-TEV peptides cleaved off from the G_5-DARPin and the G-His peptide from the DARPin-LPETG-His cleaved off by SrtA.

Comparing the SEC-purified product 9.26-LPET-G3 with the nonpurified reaction mix, we observed that the loss of antiproliferative activity at low dilutions was prevented (**Fig. 3C**). Next, when we spiked the genetic fusion construct 9.26-L1-G3 with the coupling reaction mix, we could reproduce the partial loss of antiproliferative activity at low dilutions, whether or not the reaction contained SrtA (**Fig. 3C**). Therefore, we conclude that the noncoupled monovalent DARPins compete for receptor binding with the bivalent constructs. Note that we found no evidence for an antagonistic function of SrtA itself, as the cell viability with and without SrtA is indistinguishable (**Fig. 3C**). Thus, a wide concentration window is in place to determine the antiproliferative activity directly in the reaction mixes, within which active bivalent binder combinations can be robustly identified.

Screening for active bispecific DARPins

We expressed 21 DARPins binding to EGFR, ErbB2, ErbB3, ErbB4, EpCAM, and c-MET (Supplementary Fig. S3A–S3C) in the two different formats (DARPin-LPETG and G_5-DARPin) in 2 L cultures of *E. coli* XL1-blue. We performed a standard IMAC purification for tissue culture applications (35), which efficiently removes endotoxins. Next, we enzymatically coupled all combinations of the 21 N-terminal binders to the 21 C-terminal binders to generate a matrix of 441 unique bivalent molecules. To characterize coupling efficacy, we randomly sampled coupling reactions by SDS-PAGE. We observed formation of the desired bivalent coupling products in all sampled reactions at the expected molecular weight, which shows that wtSrtA coupling is robust and homogeneous across the tested samples (Supplementary Fig. S4). Next, we treated two ErbB2-overexpressing breast cancer cell lines (BT474 and SKBR3) with three different dilutions of the coupling reaction mix in triplicates. Assuming an average coupling efficiency of at least 50%–70%, the applied dilutions of 40-, 160-, and 640-fold should correspond to a final minimal concentration of approximately 500 nmol/L, 125 nmol/L, and 3 nmol/L of bispecific DARPins, respectively.

Continuous treatment with coupling reactions mixes for 4 days showed several hits indicating significant inhibition and also some showing stimulation of cell proliferation of BT474 and SKBR3 cells in the XTT cell viability assays (**Fig. 4**). These results are presented as mean response in a heatmap (percent viability compared with that after treatment with the nonbinding control off7-LPET-off7) across all three dilutions (500 nmol/L, 125 nmol/L, and 3 nmol/L). For individual concentrations, please see Supplementary Figs. S5 and S6. Overall, the two ErbB2-overexpressing cancer cell lines showed a similar pattern of inhibition and stimulation of cell proliferation

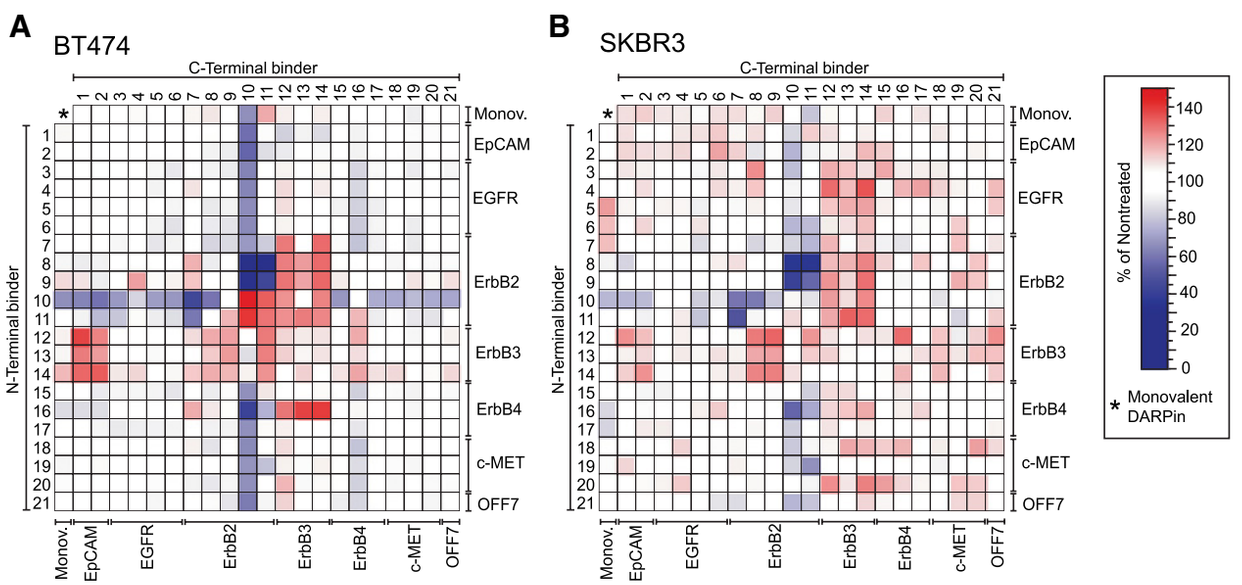

Figure 4.
Percentage of viable cells of BT474 (**A**) and SKBR3 (**B**) in color-coded heatmap representation: inhibition (blue), noneffective (white), and stimulation (red) of cell proliferation. Heatmaps show the mean of all three dilutions (40-, 160-, and 640-fold; each in triplicate). Numbers (IDs) on the left and top correspond to specific monovalent DARPins binding to the indicated receptors at the right and bottom, respectively. Off7 (ID 21) represents a non-receptor binding DARPin control. The list with assay IDs and the corresponding DARPins with references is shown in Supplementary Fig. S3A.

(**Fig. 4**). As expected, in both cell lines we identified the same biparatopic anti-ErbB2 DARPins with strong antiproliferative activity (red), such as 926E-H14 (coupling ID 8-10), 926E-G3 (ID 8-11), or 929-H14 (ID 9-10). Because these biparatopic DARPins have been described before to show strong antiproliferative effect as genetic fusions (18, 21, 36), these findings corroborate the validity of our screening method. The robustness of the SrtA-based strategy is underlined by the fact that the orientation effect of the HER2 binders is fully replicated from the genetic fusions: to induce the signaling-inactive cross-link, the N-terminal binder must engage domain 1 of the ECD, while the C-terminal binder must engage domain 4 (18, 21).

Furthermore, we identified bispecific anti-ErbB2 DARPins with strong growth-stimulating activity (blue) such as G3-G3 or H14-H14 (IDs 10 and 11) that had also been previously found as genetic fusions (18). In these cases, from the location of the epitope on domain 4 (21), the binders can probably enhance and stabilize the formation of canonical signaling–competent homodimers of ErbB2, both in the genetic fusion and in the SrtA-mediated dimer.

Besides these known constructs, we identified a series of novel bispecific DARPins with significant effects on cell proliferation. Notably, almost all combinations of DARPins simultaneously binding to ErbB2 and ErbB3 (IDs 13-11, 13-8, 14-11, 8-14) as well as pairs of anti-ErbB4 and anti-ErbB3 DARPins (IDs 16-12, 16-13, 16-14) showed a marked stimulation of cell proliferation in both cell lines. These findings reflect the strong dependence of the ErbB2-overexpressing cancer cell lines used on ErbB2-ErbB3 heterodimers for cell growth and survival (18); they potentially functionally mimic the effect of the ErbB3 ligand heregulin, although by a different molecular interaction enforcing direct linking and thus transactivation of receptor molecules. In addition, the treatment with bispecific DARPins might also promote or interfere with receptor internalization and thereby prolong receptor half-lives on the cell surface. Surprisingly, we also identified bispecific DARPins against ErbB3 and EpCAM (IDs 13-1, 13-2, 14-1, 14-2), which induced a strong stimulation of cell proliferation in BT474 cells. While EpCAM is a known signaling mediator in cancer (37), to our knowledge the potential interaction with ErbB3 has not been reported before.

Analysis of response profiles across cancer cell lines

We observed a similar picture in the overall response of SKBR3 and BT474 cells in terms of the distribution of the inhibitory and stimulatory effects across the matrix of bivalent DARPins (**Fig. 4**). This is in good agreement with their properties, as both cancer cell lines overexpress ErbB2, are highly dependent on ErbB2-signaling, and are sensitive to the mAb trastuzumab, the ErbB2 tyrosine kinase inhibitor ARRY-380, and to the biparatopic anti-ErbB2 DARPins (6L1G, 9L1H; ref. 18). Thus, we were prompted to further analyze the response profiles in more detail. For this purpose, we transformed the raw data to LFCs and compared the cell lines between the individual dilutions (40-, 160-, and 640-fold) by Pearson correlation (**Fig. 5A**). As may be expected, we observed the highest Pearson correlation coefficients (>0.9) within the same cell line between the three dilutions (**Fig. 5B**).

We observed moderately high positive Pearson correlation coefficients (> 0.5) between BT474 and SKBR3 cells, which showed that the overall response to the 441 different treatments is not identical. This finding indicates the potential of multiparameter receptor

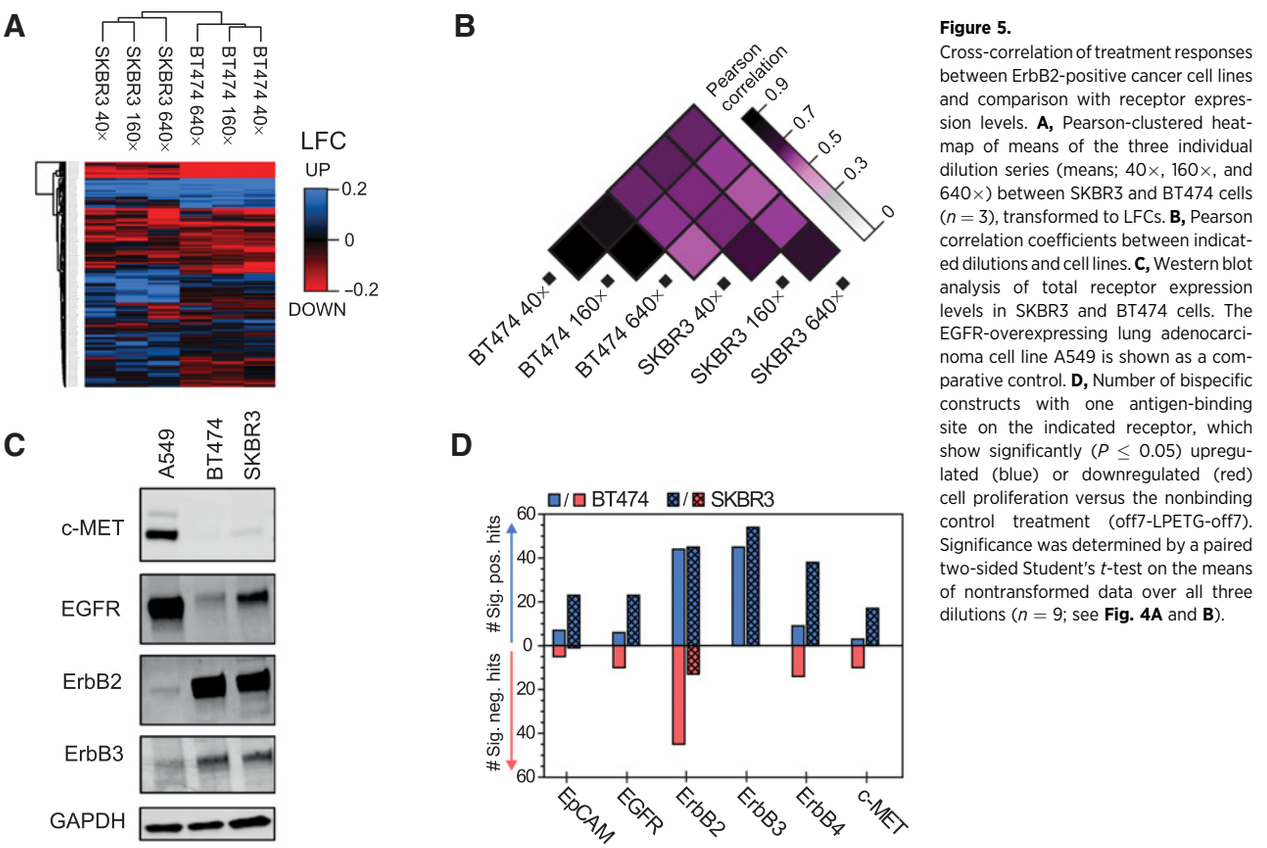

Figure 5.
Cross-correlation of treatment responses between ErbB2-positive cancer cell lines and comparison with receptor expression levels. **A,** Pearson-clustered heatmap of means of the three individual dilution series (means; 40×, 160×, and 640×) between SKBR3 and BT474 cells ($n = 3$), transformed to LFCs. **B,** Pearson correlation coefficients between indicated dilutions and cell lines. **C,** Western blot analysis of total receptor expression levels in SKBR3 and BT474 cells. The EGFR-overexpressing lung adenocarcinoma cell line A549 is shown as a comparative control. **D,** Number of bispecific constructs with one antigen-binding site on the indicated receptor, which show significantly ($P \leq 0.05$) upregulated (blue) or downregulated (red) cell proliferation versus the nonbinding control treatment (off7-LPETG-off7). Significance was determined by a paired two-sided Student's *t*-test on the means of nontransformed data over all three dilutions ($n = 9$; see **Fig. 4A** and **B**).

treatment analyses to characterize the phenotypic properties and potential targeting opportunities of different cancer cell lines, complementing the information available from RNA sequencing. Therefore, we compared the number of significant hits for a particular receptor (inhibitory or stimulatory response colored as in **Fig. 4**) with the corresponding receptor expression levels. For this purpose, we assessed total receptor expression levels by Western blotting (**Fig. 5C**) and plotted the number of significant ($P \leq 0.05$) stimulatory and inhibitory hits found in the screenings involving at least one binding paratope of the bivalent construct to this particular receptor (**Fig. 5D**). While SKBR3 and BT474 showed similar levels of total ErbB2, SKBR3 showed higher expression levels of EpCAM, EGFR, ErbB3, and c-MET. In agreement, we observed more inhibitory hits involving EpCAM, EGFR, ErbB3, and c-MET in SKBR3 cells (**Fig. 5C**). Thus, the overall number of significant growth-stimulatory and growth-inhibitory treatment hits appears to reflect the receptor expression levels, which in turn may indicate those receptors that contribute to the control of growth and proliferation in these cell lines. Therefore, this response-profiling analysis, orthogonal to Western blotting or RNA sequencing, may be able to assess functional receptor expression levels and potential targeting opportunities, even if no natural receptor dimer-selective ligands are available.

Discussion

Hallmarks of cancer cells such as enhanced proliferation, survival, and motility are frequently correlated with dysregulation of receptor expression levels, in particular those of RTKs. These receptors typically do not function in an isolated manner, but rather—as is largely the case for the proteins involved in downstream signaling—form functional networks characterized by various interactions between different receptors. As a consequence, these receptors show a degree of redundancy regarding the activation of downstream signaling pathways. Therefore, they can compensate for the loss of function of a specific receptor after therapeutic inhibition by alternative signaling through another receptor. This makes the development of effective treatments so difficult.

Compensatory upregulation of receptor expression seems to constitute a fundamental feature of cancer cells to develop an initial resistance against targeted therapy. Therefore, next-generation–targeted therapies and personalized diagnostics have to take these phenomena into account during treatment.

Here, we specifically developed a scalable *in vitro* method to generate new bispecific binders in a highly efficient manner from individually expressed monovalent DARPins using SrtA-mediated transpeptidation. The greater their number, the more attractive this strategy becomes compared with the straight cloning and purification of individual bispecific molecules for initial screenings, as the sum of the components can generate the multiplication product of covalently linked bispecific binders.

We have shown that wtSrtA is better suited for performing a one-pot DARPin–DARPin coupling reaction, because the evolved SrtA pentamutant (33) showed an increased hydrolysis rate of the acyl–enzyme intermediate. For our application, it was not only critical to have a high absolute yield, but even more so to have as few monomers as possible in the final mixture, be it from remaining educts or from hydrolyzed acyl–enzyme intermediates. In fact, the absolute reaction rate would be of no particular importance. This favorable ratio of bispecific product over residual monomers allowed us to apply the mixtures directly to high-throughput proliferation assays on human cancer cells. The final product mixture was suitable for cell culture testing because it was generated from well-purified educts and enzymes produced in *E. coli*.

We generated 441 different bispecific binders from 21 monovalent DARPins against various epitopes on different RTKs and EpCAM, and performed a screening for the effects on cell proliferation on two ErbB2-overexpressing breast cancer cell lines. The screening identified a series of both known and novel bispecific constructs with significant inhibiting or stimulating effects on cell proliferation.

Furthermore, the combined data of all responses in our dataset revealed cell line–specific patterns in the stimulation and inhibition of cell proliferation, which could be used to characterize cancer cells in a novel functional manner. We found very strong positive Pearson correlation coefficients (≥ 0.9) within the same cancer cell line at different dilutions and moderately high positive Pearson correlation coefficients (≥ 0.5) between similar cancer cell lines. We hypothesized that the generated response profiles could be used to distinguish between cancer cell lines based on their cell surface receptor landscape, and particularly their sensitivity to stimulation or inhibition of certain receptors, in the absence of any specific kinase inhibitor or receptor-dimer–specific natural ligands.

In fact, we found that the number of significant effects on cell proliferation followed the relative expression levels of the respective receptors on these two cell lines. These findings therefore demonstrate the potential of our method to characterize cell lines based on a collection of actual biological responses. Thus, besides the discovery of particular bispecific binding agents with agonistic or antagonistic activity on cancer cell proliferation, our response analysis may represent a novel tool to functionally characterize and subtype cancer cells, based on their cell surface receptor landscape.

Disclosure of Potential Conflicts of Interest

No potential conflicts of interest were disclosed.

Authors' Contributions

Conception and design: F. Andres, M. Schwill, A. Plückthun
Development of methodology: F. Andres, M. Schwill
Acquisition of data (provided animals, acquired and managed patients, provided facilities, etc.): F. Andres, M. Schwill, Y.L. Boersma
Analysis and interpretation of data (e.g., statistical analysis, biostatistics, computational analysis): F. Andres, M. Schwill, Y.L. Boersma
Writing, review, and/or revision of the manuscript: F. Andres, M. Schwill, Y.L. Boersma, A. Plückthun
Administrative, technical, or material support (i.e., reporting or organizing data, constructing databases): F. Andres, M. Schwill
Study supervision: A. Plückthun

Acknowledgments

The authors would like to thank Dr. T.E. Adams from CSIRO Manufacturing, Melbourne, Australia, for providing the ErbB3 Fc-fusion protein. The authors would like to thank Dr. Rastislav Tamaskovic and Dr. Manuel Simon for helpful scientific discussions. This work was supported by the Schweizerischer Nationalfonds (grant no. 310030B_166676; to A. Plückthun) and Rubicon postdoctoral grant 680-50-0704 from the Dutch Organization for Scientific Research (NWO; to Y.L. Boersma).

The costs of publication of this article were defrayed in part by the payment of page charges. This article must therefore be hereby marked *advertisement* in accordance with 18 U.S.C. Section 1734 solely to indicate this fact.

Received July 1, 2019; revised September 6, 2019; accepted December 13, 2019; published first December 23, 2019.

References

1. Ekman D, Björklund AK, Frey-Skott J, Elofsson A. Multi-domain proteins in the three kingdoms of life: orphan domains and other unassigned regions. J Mol Biol 2005;348:231–43.
2. Rolland T, Tasan M, Charloteaux B, Pevzner SJ, Zhong Q, Sahni N, et al. A proteome-scale map of the human interactome network. Cell 2014;159: 1212–26.
3. Pincet F. Membrane recruitment of scaffold proteins drives specific signaling. PLoS One 2007;2:e977.
4. Luo LY, Hahn WC. Oncogenic signaling adaptor proteins. J Genet Genomics 2015;42:521–9.
5. Gherardi E, Youles ME, Miguel RN, Blundell TL, Iamele L, Gough J, et al. Functional map and domain structure of MET, the product of the c-met protooncogene and receptor for hepatocyte growth factor/scatter factor. Proc Natl Acad Sci U S A 2003;100:12039–44.
6. Turner N, Grose R. Fibroblast growth factor signalling: from development to cancer. Nat Rev Cancer 2010;10:116–29.
7. Ko B, He T, Gadgeel S, Halmos B. MET/HGF pathway activation as a paradigm of resistance to targeted therapies. Ann Transl Med 2017;5:4.
8. Usmani SS, Bedi G, Samuel JS, Singh S, Kalra S, Kumar P, et al. THPdb: Database of FDA-approved peptide and protein therapeutics. PLoS One 2017;12: e0181748.
9. Bordeaux J, Welsh A, Agarwal S, Killiam E, Baquero M, Hanna J, et al. Antibody validation. Biotechniques 2010;48:197–209.
10. Harris LJ, Skaletsky E, McPherson A. Crystallographic structure of an intact IgG1 monoclonal antibody. J Mol Biol 1998;275:861–72.
11. Ahmad S, Gupta S, Kumar R, Varshney GC, Raghava GP. Herceptin resistance database for understanding mechanism of resistance in breast cancer patients. Sci Rep 2014;4:4483.
12. Villamor N, Montserrat E, Colomer D. Mechanism of action and resistance to monoclonal antibody therapy. Semin Oncol 2003;30:424–33.
13. Brand TM, Iida M, Wheeler DL. Molecular mechanisms of resistance to the EGFR monoclonal antibody cetuximab. Cancer Biol Ther 2011;11: 777–92.
14. Kontermann RE, Brinkmann U. Bispecific antibodies. Drug Discov Today 2015; 20:838–47.
15. Krishnamurthy A, Jimeno A. Bispecific antibodies for cancer therapy: a review. Pharmacol Ther 2018;185:122–34.
16. Jost C, Plückthun A. Engineered proteins with desired specificity: DARPins, other alternative scaffolds and bispecific IgGs. Curr Opin Struct Biol 2014;27: 102–12.
17. Plückthun A. Designed ankyrin repeat proteins (DARPins): binding proteins for research, diagnostics, and therapy. Annu Rev Pharmacol Toxicol 2015;55: 489–511.
18. Tamaskovic R, Schwill M, Nagy-Davidescu G, Jost C, Schaefer DC, Verdurmen WP, et al. Intermolecular biparatopic trapping of ErbB2 prevents compensatory activation of PI3K/AKT via RAS-p110 crosstalk. Nat Commun 2016;7:11672.
19. Stefan N, Martin-Killias P, Wyss-Stoeckle S, Honegger A, Zangemeister-Wittke U, Plückthun A. DARPins recognizing the tumor-associated antigen EpCAM selected by phage and ribosome display and engineered for multivalency. J Mol Biol 2011;413:826–43.
20. Boersma YL, Chao G, Steiner D, Wittrup KD, Plückthun A. Bispecific designed ankyrin repeat proteins (DARPins) targeting epidermal growth factor receptor inhibit A431 cell proliferation and receptor recycling. J Biol Chem 2011;286: 41273–85.
21. Jost C, Schilling J, Tamaskovic R, Schwill M, Honegger A, Plückthun A. Structural basis for eliciting a cytotoxic effect in HER2-overexpressing cancer cells via binding to the extracellular domain of HER2. Structure 2013; 21:1979–91.
22. Schaefer G, Haber L, Crocker LM, Shia S, Shao L, Dowbenko D, et al. A two-in-one antibody against HER3 and EGFR has superior inhibitory activity compared with monospecific antibodies. Cancer Cell 2011;20:472–86.
23. Steiner D, Forrer P, Plückthun A. Efficient selection of DARPins with sub-nanomolar affinities using SRP phage display. J Mol Biol 2008;382:1211–27.
24. Zahnd C, Pecorari F, Straumann N, Wyler E, Plückthun A. Selection and characterization of Her2 binding-designed ankyrin repeat proteins. J Biol Chem 2006;281:35167–75.
25. Zahnd C, Wyler E, Schwenk JM, Steiner D, Lawrence MC, McKern NM, et al. A designed ankyrin repeat protein evolved to picomolar affinity to Her2. J Mol Biol 2007;369:1015–28.
26. Andres F, Iamele L, Meyer T, Stüber JC, Kast F, Gherardi E, et al. Inhibition of the MET kinase activity and cell growth in MET-addicted cancer cells by bi-paratopic linking. J Mol Biol 2019;431:2020–39.
27. Mao H, Hart SA, Schink A, Pollok BA. Sortase-mediated protein ligation: a new method for protein engineering. J Am Chem Soc 2004;126:2670–1.
28. Mazmanian SK, Liu G, Ton-That H, Schneewind O. Staphylococcus aureus sortase, an enzyme that anchors surface proteins to the cell wall. Science 1999; 285:760–3.
29. Binz HK, Amstutz P, Kohl A, Stumpp MT, Briand C, Forrer P, et al. High-affinity binders selected from designed ankyrin repeat protein libraries. Nat Biotechnol 2004;22:575–82.
30. Sugiyama A, Umetsu M, Nakazawa H, Niide T, Onodera T, Hosokawa K, et al. A semi high-throughput method for screening small bispecific antibodies with high cytotoxicity. Sci Rep 2017;7:2862.
31. Kontermann RE. Dual targeting strategies with bispecific antibodies. MAbs 2012; 4:182–97.
32. Dreier B, Plückthun A. Rapid selection of high-affinity binders using ribosome display. Methods Mol Biol 2012;805:261–86.
33. Chen I, Dorr BM, Liu DR. A general strategy for the evolution of bond-forming enzymes using yeast display. Proc Natl Acad Sci U S A 2011;108:11399–404.
34. Clancy KW, Melvin JA, McCafferty DG. Sortase transpeptidases: insights into mechanism, substrate specificity, and inhibition. Biopolymers 2010;94:385–96.
35. Tamaskovic R, Simon M, Stefan N, Schwill M, Plückthun A. Designed ankyrin repeat proteins (DARPins) from research to therapy. Methods Enzymol 2012; 503:101–34.
36. Schwill M, Tamaskovic R, Gajadhar AS, Kast F, White FM, Plückthun A. Systemic analysis of tyrosine kinase signaling reveals a common adaptive response program in a HER2-positive breast cancer. Sci Signal 2019;12. doi: 10.1126/scisignal.aau2875.
37. Munz M, Baeuerle PA, Gires O. The emerging role of EpCAM in cancer and stem cell signaling. Cancer Res 2009;69:5627–9.